CHEMISTRY
A EUROPEAN JOURNAL

DOI: 10.1002/chem.200601279

Ferromagnetism in a New Manganese-Related Brownmillerite: $La_{0.5}Sr_{0.5}MnO_{2.5}$

Raquel Cortés-Gil,[a, b] M. Luisa Ruiz-González,[a] José M. Alonso,[b, c] María Vallet-Regí,[b, d] Antonio Hernando,[b, e] and José M. González-Calbet*[a, b]

Abstract: The topotactic reduction of $La_{0.5}Sr_{0.5}MnO_3$ leads to ordering of the anionic vacancies in the $La_{0.5}Sr_{0.5}MnO_{2.5}$ composition. The isolated material, which is isostructural with $Sr_2Fe_2O_5$, crystallises in the brownmillerite structural type with unit cell parameters $a=0.54117(3)$, $b=1.67608(12)$, $c=0.54004(3)$ nm and space group *Ibm*2. Its microstructural characterisation by means of electron diffraction and high-resolution electron microscopy suggests a complex microstructure arising from the coherent intergrowth of different brownmillerite-type domains that show short-range ordering at the A sub-lattice. The layer structure of $La_{0.5}Sr_{0.5}MnO_{2.5}$ leads to a double magnetic behaviour where a ferromagnetic two-dimensional component is present.

Keywords: electron diffraction · electron microscopy · magnetic properties · manganese · mixed-valent compounds

Introduction

Much of the research effort devoted to manganese-related perovskites ($AMnO_3$) has been triggered by the need to understand the origin of their so-called colossal magnetoresistance.[1] The paramount role played by the concentration of doped holes (Mn^{4+}) in $Ln_{1-x}D_xMnO_3$ (Ln: lanthanide; D: divalent ion) was recognised early on, and the influence of compositional variations in the A sub-lattice has been widely studied since D ions provide holes to the band[2–5] and act as effective attractors for these holes.[6,7] It has also been shown that disorder effects due to size differences between the Ln and D cations play an important role in magnetoresistant perovskites.[8,9] Magnetic interactions in the above system depend on the value of x, with the Mn^{3+}–O–Mn^{4+} exchange interaction being ferromagnetic, since the e_g itinerant electron is exchanged between Mn^{3+} and Mn^{4+} by a double-exchange mechanism,[10] whereas Mn^{3+}–O–Mn^{3+} and Mn^{4+}–O–Mn^{4+} couplings due to superexchange interactions of opposite sign give rise, generally, to antiferromagnetic structures.[11–13] Particular attention has been focused on the behaviour around $x=0.5$ in the magnetic phase diagram of $La_{1-x}D_xMnO_3$, where, when D is calcium, the ground state changes from a ferromagnetic to an antiferromagnetic insulator and is associated with a charge-ordering state[14–16] in which doped Mn^{4+} holes are electrostatically locked into a periodic array and are not able to become involved in any conduction mechanism.[17] However, when D is strontium the phase diagram reveals that the competition between the ferromagnetic double-exchange and antiferromagnetic charge-ordering instability gives rise to a lattice-coupled first-order phase transition induced by a relatively low magnetic field.[18]

Compositional variations in the anionic sub-lattice of manganites have been much less studied despite the fact that a large number of anion-deficient perovskite-related superstructures, due to unoccupied oxygen position ordering, have been reported in other systems. Low-temperature reduction routes have been shown to be effective in promoting

[a] R. Cortés-Gil, Dr. M. L. Ruiz-González, Prof. J. M. González-Calbet
Departamento de Química Inorgánica
Facultad de Químicas, Universidad Complutense de Madrid
28040 Madrid (Spain)
Fax: (+34) 91-394-4342
E-mail: jgcalbet@quim.ucm.es

[b] R. Cortés-Gil, Dr. J. M. Alonso, Prof. M. Vallet-Regí, Prof. A. Hernando, Prof. J. M. González-Calbet
Instituto de Magnetismo Aplicado, UCM-CSIC-ADIF
Las Rozas, P.O. Box 155, 28230 Madrid (Spain)

[c] Dr. J. M. Alonso
Instituto de Ciencia de Materiales, CSIC
Sor Juana Inés de la Cruz s/n, 28049 Madrid (Spain)

[d] Prof. M. Vallet-Regí
Departamento de Química Inorgánica y Bioinorgánica
Facultad de Químicas, Universidad Complutense de Madrid
28040 Madrid (Spain)

[e] Prof. A. Hernando
Departamento de Física de Materiales, Facultad de Físicas
Universidad Complutense de Madrid, 28040 Madrid (Spain)

oxygen vacancy ordering in perovskite-related oxides,[19,20] and several oxygen vacancy patterns that lead to different polyhedral types have been described for manganese-containing compounds. the topotactic reduction of $CaMnO_3$, for instance, converts MnO_6 octahedra into MnO_5 square pyramids due to alternate vacancy ordering along the $[101]_c$ direction (c stands for cubic perovskite). This leads to $CaMnO_{2.5}$[21] and other intermediate $CaMnO_{3-\delta}$ superstructures where Mn^{4+} and Mn^{3+} coexist.[21,22] A different perovskite-related superstructure with Mn in a square-pyramidal coordination has been reported by Millange et al.[23] for $LaBaMn_2O_5$; it is isostructural to $YBaCuFeO_5$[24] with alternate vacancy ordering along $[010]_c$. Ordering along $[101]_c$ in alternate layers along the *b* direction takes place when $La_{0.5}Ca_{0.5}MnO_3$ perovskite is reduced to $La_{0.5}Ca_{0.5}MnO_{2.5}$, which leads to a material with a brownmillerite-related structure that can be described as an alternating sequence of octahedral and tetrahedral layers along the *b* direction of the perovskite subcell[25] (Figure 1). The introduction of anionic vacancies must necessarily affect both the structural and magnetic properties. It is well known that $La_{0.5}Ca_{0.5}MnO_3$ exhibits a transition from paramagnetic to an almost ferromagnetic state at a temperature of around 254 K and a clear drop in the susceptibility due to charge ordering of the charge carriers at 190 K.[26] However, oxygen deficiency produces a gradual decrease in the magnetic susceptibility of the $La_{0.5}Ca_{0.5}MnO_{3-\delta}$ system for δ values above 0.20 and a much larger decrease for a δ value of 0.50.[25] Although preliminary studies suggest that the anion deficiency is a consequence of the coexistence of Mn^{4+} and Mn^{2+}, a detailed X-ray absorption near-edge spectroscopy (XANES) and thermogravimetric study[27] has suggested that 12.5% of Mn^{4+} coexists with Mn^{3+} and Mn^{2+} in the coordination polyhedron. Very recently, charge- and structural-ordering has been described in the brownmillerite phases $La_{1-x}Sr_xMnO_{2.5}$ ($0.2 < x < 0.4$), although the magnetic and electric properties were not measured.[28]

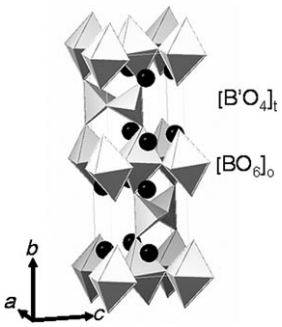

Figure 1. $A_2BB'O_5$ brownmillerite structural model along [001] showing the B and B′ coordination polyhedra; the circles represent the A cations.

Modification of the $[CaO_{12}]$ and $[SrO_{12}]$ polyhedra introduces some distortions in the Mn^{3+}–O–Mn^{4+} angles due to the different radii of the D cations,[29] which are responsible for dramatic changes, especially for $x = 0.5$, in the magnetic phase diagrams[30,31] of both $La_{1-x}Sr_xMnO_3$ and $La_{1-x}Ca_xMnO_3$ systems. On the basis of this information, we have undertaken a study of the influence of the oxygen deficiency in the $La_{0.5}Sr_{0.5}MnO_{3-\delta}$ system. We report here a study of the ordering of anionic vacancies in $La_{0.5}Sr_{0.5}MnO_{2.5}$ by means of X-ray and selected-area electron diffraction (SAED) and high-resolution electron microscopy (HREM) and its influence on the magnetic behaviour.

Results and Discussion

The powder X-ray diffraction (XRD) pattern corresponding to $La_{0.5}Sr_{0.5}MnO_{2.5}$ (Figure 2) is similar to that obtained for $La_{0.5}Ca_{0.5}MnO_{2.5}$.[25] It can be indexed on the basis of a relat-

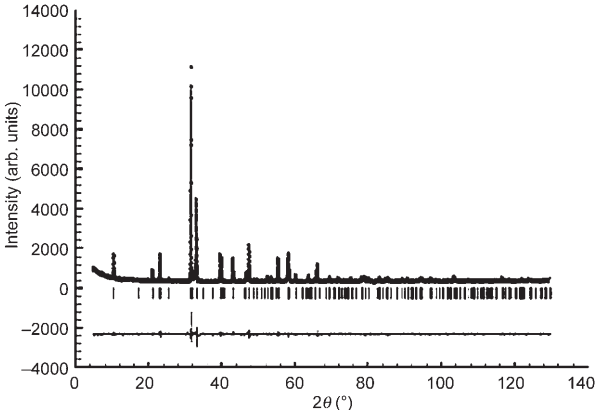

Figure 2. Graphic result of the fitting of the powder XRD data of $La_{0.5}Sr_{0.5}MnO_{2.5}$: experimental (points), calculated (solid line) and difference (bottom).

ed brownmillerite unit cell (*Ibm*2) with lattice parameters $a = 0.54117(3)$, $b = 1.67608(12)$, $c = 0.54004(3)$ nm, which suggest a slightly smaller orthorhombic distortion compared to the calcium phase, probably due to the effect of the bigger size of Sr with respect to Ca. Rietveld profile refinement of the XRD pattern was done with the model of the $Sr_2Fe_2O_5$ brownmillerite-related structure that crystallises in the space group *Ibm*2.[32] The profile refinement done with these coordinates resulted in a satisfactory agreement with the calculated and experimental (*hkl*) values, with $R_p = 4.86$, $R_{w,p} = 6.41$ and $R_B = 7.68$. The small differences between the calculated and experimental intensities for the (114) reflection can be explained on the basis of preferential orientation. The final structural parameters are collected in Table 1, and some selected interatomic distances are gathered in Table 2. The high value of the isotropic temperature factors (*B*) corresponding to Mn(2) and O(3), which are the manganese and equatorial oxygen atoms at the tetrahedral sites, suggests a possible disorder phenomena. We should point out at this point that brownmillerite compounds generally crystallise in either the *Ibm*2[32] or *Pnma*[33] space group. However, there are also a few papers[33–36] that report a better fit of the Rietveld refinement using the *Icmm* space group as a consequence of order/disorder phenomena. In fact, SAED studies with $Ba_2In_2O_5$[35] and $Sr_2Co_{2-x}Ga_xO_5$[36] have revealed the appearance of diffuse streaking along certain directions, which confirms the presence of order/disorder phenomena. In the *Icmm* space group, the 8i sites corresponding to the

Table 1. Final structural parameters of $La_{0.5}Sr_{0.5}MnO_{2.5}$.[a]

Atom	*x*/*a*	*y*/*b*	*z*/*c*	*B* [Å^2]	Occupancy
Mn(1)	0.00000(0)	0.00000(0)	0.00000(0)	0.71 (1)	0.5
Mn(2)	−0.043(2)	0.25000(0)	−0.053(3)	1.28(2)	0.5
La/Sr	−0.0009(9)	0.11184(8)	0.500(3)	0.24(2)	0.5
O1	0.27965(0)	0.006(2)	0.254(5)	0.24(3)	1
O2	0.006(6)	0.1357(6)	0.0358(7)	0.24(3)	1
O3	1.014(9)	0.25000(0)	0.482(9)	6.41(8)	0.5

[a] Space group *Ibm*2 (123); $a=0.54117(3)$, $b=1.67608(12)$, $c=0.54004(3)$ nm; $R_{wp}=0.0641$, $R_B=0.0768$, $R_p=0.0486$, $\chi^2=0.0165$.

Table 2. Selected interatomic distances [Å] and angles [°] in $La_{0.5}Sr_{0.5}MnO_{2.5}$.

Mn(1)−O(1)	2.04(2) (×2)	La/Sr−O(1)	2.82(3)
Mn(1)−O(1)	1.78(3) (×2)	La/Sr−O(1)	2.69(3)
Mn(1)−O(2)	2.279(1) (×2)	La/Sr−O(1)	2.67(4)
Mn(2)−O(2)	1.95(1) (×2)	La/Sr−O(1)	2.544(4)
Mn(2)−O(3)	2.56(8)	La/Sr−O(2)	2.64(6)
Mn(2)−O(3)	2.89(8)	La/Sr−O(2)	2.82(6)
Mn(2)−O(3)	2.89(5)	La/Sr−O(2)	2.52(3)
Mn(2)−O(3)	2.52(5)	La/Sr−O(2)	2.94(3)
		La/Sr−O(3)	2.34(8)
Mn(1)-O(1)-Mn(1)	173.388	Mn(2)-O(3)-Mn(2)	164.796

metal lying at the tetrahedral position and one of the oxygen atoms [O(3)] have mean occupancies of one half, which allows disordered displacements of these atoms. This situation can also be understood on the basis of disorder configurations of the tetrahedral layers in both *Ibm*2 and *Pnma* space groups that are characteristic of the brownmillerite structure.[37] All three of these orthorhombic space groups were initially considered in the refinement; the best results were obtained with *Ibm*2. Moreover, the SAED studies are in agreement with this space group, as discussed below.

To investigate possible order/disorder phenomena that are usually present in oxygen-deficient perovskite-related phases, a microstructural characterisation by means of

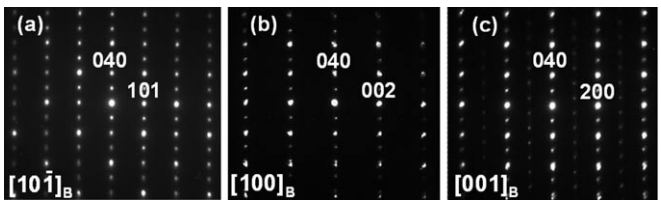

Figure 3. SAED patterns along the zone axes $[10\bar{1}]_B$ (a), $[100]_B$ (b) and $[001]_B$ (c).

SAED and HREM was performed. Figure 3 shows the SAED patterns along the $[10\bar{1}]_B$, $[100]_B$ and $[001]_B$ zone axes (B stands for the brownmillerite cell), which are in agreement with the XRD data. The HREM image corresponding to the $[10\bar{1}]_B$ zone axis is shown in Figure 4a. The situation seems to be more complex since several domains with different periodicities, marked as A and B, are apparent. Area A shows interlayer distances in accordance with the brownmillerite cell along the $[10\bar{1}]_B$ zone axis. This is also reflected in the corresponding fast Fourier transform (FFT; Figure 4b), which is identical to the experimental one. Area B, which lies close to the edge of the crystal, exhibits a periodicity of 0.38×0.38 nm, which is characteristic of the brownmillerite cell along $[010]_B$, parallel to the $[001]_c$ projection of the cubic perovskite sub-lattice, and therefore suggests the presence of perpendicular domains. This is again reflected in the corresponding FFT (Figure 4c). Note that the overlap of both these FFTs fits well with the experimental pattern (Figure 3a). A good agreement between the experimental images and those calculated taking into account the brownmillerite cell, which are inserted in each domain, is observed.

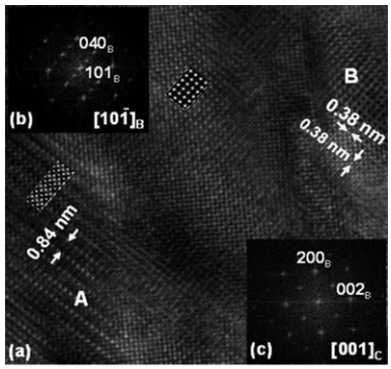

Figure 4. a) HREM image along $[10\bar{1}]_B$ showing domains A and B. Calculated images of each domain are included; b) FFT corresponding to domain A; c) FFT corresponding to domain B.

Figure 5a shows an HREM image along $[100]_B$, which is titled by 45° with respect to the $[10\bar{1}]_B$ axis. Once again, two different domains are clearly observed. Domain A shows periodicities of 0.84 and 0.27 nm, in agreement with the $[100]_B$ projection of the brownmillerite cell. An enlargement of domain A, including the calculated image, is shown in Figure 5b. A good agreement between the experimental and

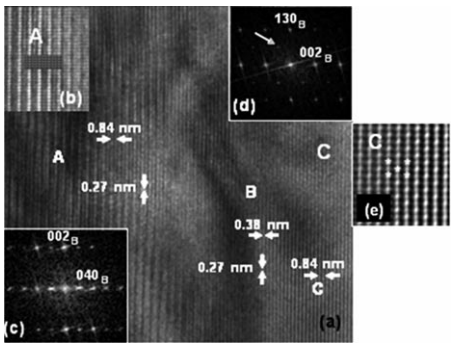

Figure 5. a) HREM image along $[100]_B$; b) enlargement of domain A and its corresponding calculated image; c) FFT corresponding to domain A; d) FFT corresponding to domain B; e) enlargement of area C in domain B and filtered image of area C.

calculated images is again observed. The FFT corresponding to this domain is shown in Figure 5c, which nicely fits the experimental pattern depicted in Figure 3b. Domain B shows periodicities of 0.38×0.27 nm, and the corresponding FFT (Figure 5d) can be indexed on the basis of the $[10\bar{1}]_B$ projection of the brownmillerite cell parallel to the $[10\bar{1}]_c$ projection of the cubic perovskite sub-lattice. It is worth mentioning that a periodicity of 0.84 nm is also observed in isolated areas (marked C) of domain B. The corresponding FFT shows a very weak spot doubling the $(111)_c//(132)_B$ and equivalent directions (indicated with an arrowed in Figure 5d), which is not allowed in the brownmillerite-type space group, along with the reflections characteristic of the $[10\bar{1}]_c$ projection,. This additional order is more clearly observed in Figure 5e, which is a filtered image of area C obtained by applying masks to the FFT shown in Figure 5c. Double distances along $[010]_c//[310]_B$ are clearly seen. This local phenomenon cannot be appreciated by XRD but only with a lower wavelength technique such as electron diffraction. This situation is characteristic of a double cell along the three basic directions and is a local phenomenon that has already been described in several related $AA'BB'O_6$ perovskites where two cations are available for the A and/or B lattice positions.[38,39]

Taken together, these results indicate that $La_{0.5}Sr_{0.5}MnO_{2.5}$ is a new brownmillerite phase that exhibits a complex microstructure due to the coherent intergrowth of different domains that show short-range ordering in the A sub-lattice.

As mentioned above, the introduction of anionic vacancies strongly modifies the magnetic behaviour of the AFM parent perovskite material in the Ca-doped system. The influence of oxygen deficiency in FM $La_{0.5}Sr_{0.5}MnO_3$ must therefore also be considered. Figure 6a shows the variation of the magnetisation versus the magnetic field at several temperatures. Two different behaviours can be clearly observed. At low magnetic field, a sharp hysteresis loop with a relatively high coercive field whose value decreases as the temperature increases appears (Table 3). Although this behaviour is characteristic of ferromagnetic materials, it is worth recalling that the loop does not reach saturation since the magnetisation changes linearly with the applied field in the high-field region (2-5 T range). This behaviour indicates that there is a second contribution to the total magnetisation which, according to the observed values, must be AFM. The inset in Figure 6a shows that the ZFC and FC curves are different. This suggests a magnetic disorder, which can be understood on the basis of the coexistence of the two magnetic behaviours. It is worth mentioning that charge ordering is not detected, which is not surprising since the parent $La_{0.5}Sr_{0.5}MnO_3$ material is FM.[31] The isostructural material $La_{0.5}Ca_{0.5}MnO_{2.5}$ was also studied for comparison. Figure 6b shows the variation of the magnetisation versus the magnetic field at the same temperatures. A noticeable change is observed, since only an AFM contribution appears in the whole temperature range. To gain further understanding, the two magnetic contributions of the Sr-doped sample were studied independently.

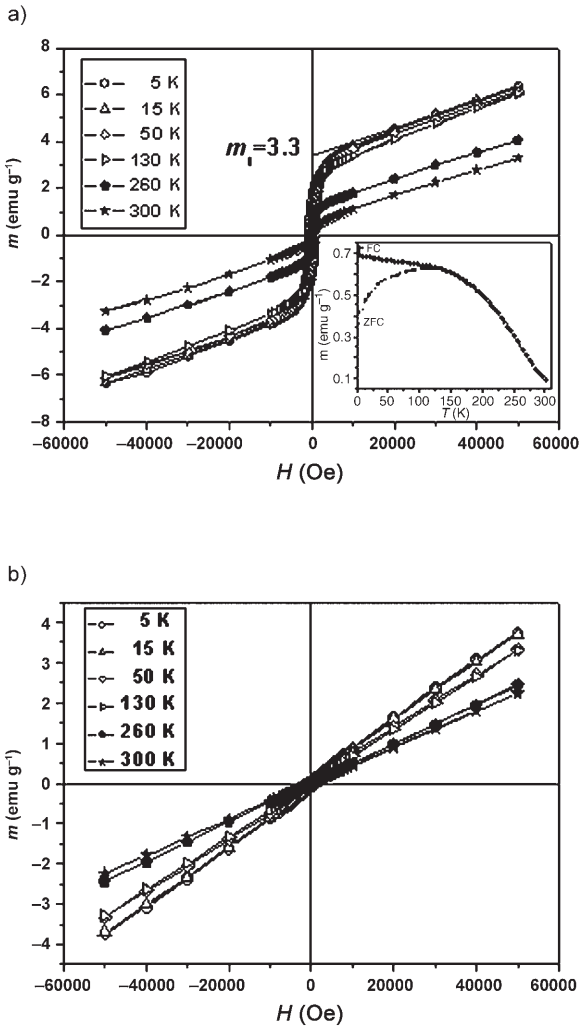

Figure 6. a) Magnetisation curve of $La_{0.5}Sr_{0.5}MnO_{2.5}$ as a function of the magnetic field. The thermal dependence of the magnetisation (applied field: 1000 Oe) is shown in the inset; b) magnetisation curve of $La_{0.5}Ca_{0.5}MnO_{2.5}$ as a function of the magnetic field.

Table 3. Coercive field (H_c) saturation magnetisation (m_s) of $La_{0.5}Sr_{0.5}MnO_{2.5}$ as a function of temperature.

T [K]	H_c [Oe]	m_s [emu g^{-1}]
5	704	3.3
15	601	3.3
50	457	3.2
130	271	2.8
260	54	1.3
300	13	0.67

The ferromagnetic contribution can be obtained by subtracting the linear behaviour shown by the magnetisation in the high-field region. A saturation magnetisation (m_s) of 3.3 emu g^{-1} is obtained at 5 K and 0.67 emu g^{-1} at room temperature. The AFM contribution is obtained by subtracting the FM contribution from the total. The magnetisation value thus obtained for the highest applied field is 3.0 emu g^{-1} at 5 K (Figure 7a). A similar behaviour is ob-

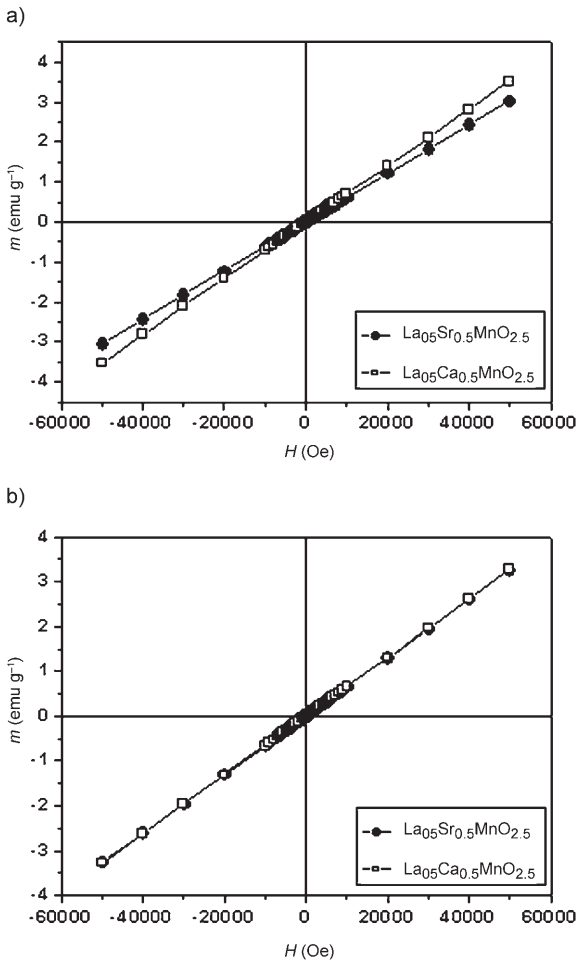

Figure 7. Comparison of the AFM contribution corresponding to $La_{0.5}Sr_{0.5}MnO_{2.5}$ and $La_{0.5}Ca_{0.5}MnO_{2.5}$ at 5 K (a) and 130 K (b). The FM contribution in the Sr doped sample has been subtracted.

served for the Ca-doped sample (Figure 7a). It is worth mentioning that the AFM contribution shows a similar behaviour over the whole temperature range for both Ca- and Sr-doped brownmillerite-type materials; the behaviour at 130 K is depicted in Figure 7b.

It could be supposed that the FM contribution is related to the presence of a small percentage of non-reduced starting material. At this point, it is worth stressing that $La_{0.5}Sr_{0.5}MnO_{2.5}$ shows a Curie temperature of 260 K, which is lower than that for $La_{0.5}Sr_{0.5}MnO_3$ (315 K). Moreover, $La_{0.5}Sr_{0.5}MnO_3$ shows a saturation magnetisation of 72 emu g^{-1} at 5 K, whereas it is 3.3 emu g^{-1} for $La_{0.5}Sr_{0.5}MnO_{2.5}$. This would mean that around 5% of an $La_{0.5}Sr_{0.5}MnO_3$ impurity phase is responsible for the FM contribution. This possibility can be discarded since such a quantity of non-reduced phase should be clearly detected by XRD. Moreover, if the experimental average composition is $O_{2.5}$ per unit formula, the presence of 5% of non-reduced sample should be accompanied by other reduction products, which are not observed either in the experimental XRD pattern or the TEM study (SAED and X-ray energy dispersive spectroscopy (XEDS)).

A double magnetic behaviour has been reported previously for other brownmillerite-related materials such as $Ca_2Fe_2O_5$. Although most of these materials show a G-type AFM behaviour,[35] Marchukov et al.[40] have concluded that the dicalcium ferrite provides a very interesting possibility for this layered structure to be treated as two canted antiferromagnets by putting one into the other with an antiferromagnetic interaction between the weak ferromagnetic components. Its magnetisation curve suggests a rather small ferromagnetic component (0.67 emu g^{-1} at 20 K) which is more than one order of magnitude smaller than that observed in $La_{0.5}Sr_{0.5}MnO_{2.5}$. This important difference suggests that spin canting is not the origin of the ferromagnetism in our Mn-related brownmillerite.

The fact that the structures, anionic compositions, vacancy ordering and antiferromagnetic contributions of both Ca- and Sr-doped brownmillerite-type materials are so similar suggests that the origin of the different magnetic behaviour resides in the different configuration of the A cationic sublattice. In fact, the well-known parent materials $La_{0.5}Ca_{0.5}MnO_3$ and $La_{0.5}Sr_{0.5}MnO_3$ are CE-type antiferromagnetic[9] and ferromagnetic,[28] respectively. The different distortions introduced by the divalent ion lead to a charge-ordering state in the Ca-doped sample that is not attained in the Sr one.[41] The reduced samples are prepared by a topotactic reduction route that gives rise to brownmillerite-type materials, namely a fourfold superlattice of the parent perovskite structure, and the question therefore arises as to whether the magnetic behaviour of the oxidised samples is maintained during the reduction process. The experimental results show that the Ca-doped reduced sample keeps the antiferromagnetic behaviour whereas the introduction of anionic vacancies in the Sr one keeps the ferromagnetic ordering only partially, with a double magnetic behaviour being attained. Since the introduction of anionic vacancies breaks the Mn^{3+}–O–Mn^{4+} exchange ferromagnetic interactions[42] and these vacancies are confined in the tetrahedral layers, the remaining ferromagnetism observed in the Sr sample seems to be related to exchange interactions through the octahedral layers. The smaller orthorhombic distortion observed in the Sr-doped brownmillerite material involves Mn1−O1−Mn1 angles of 173.388° (see Table 2), which are close to 180° and therefore enable double exchange interactions along the octahedral layers that lead to a two-dimensional magnetic system. At this point, it is worth remembering that, on the basis of XANES data,[27] the Ca-doped brownmillerite sample shows three Mn oxidation states according to the composition $La_{0.5}Ca_{0.5}Mn^{IV}_{0.125}Mn^{III}_{0.25}Mn^{II}_{0.625}O_{2.5}$, where Mn^{II} is presumably accommodated in the tetrahedral layers. If the Sr sample were to exhibit the same oxidation states, the octahedral layers would be occupied by 12% Mn^{IV}, 25% Mn^{III} and 12% Mn^{II}, thereby allowing an Mn^{3+}–O–Mn^{4+} double exchange interaction, whereas the tetrahedral one, which would only be occupied by Mn^{II}, would keep the antiferromagnetic behaviour. A powder

neutron diffraction study is in progress to solve the magnetic structure.

Conclusion

The topotactic reduction of $La_{0.5}Sr_{0.5}MnO_3$ leads to the stabilisation of a new brownmillerite-type material with the composition $La_{0.5}Sr_{0.5}MnO_{2.5}$. The oxygen deficiency in this material is accommodated along [101], which leads to octahedral layers alternating with tetrahedral ones along the *b* axis. SAED and HREM reveal a noticeable microstructure due to the intergrowth of perpendicular brownmillerite-type domains that show short-range ordering at the A sub-lattice. This layered material presents a double magnetic behaviour where the ferromagnetic contribution seems to be related to two-dimensional exchange interactions through the octahedral layers. Although the structural characterisation reveals short-range ordering at the A sub-lattice, which could be accompanied by some Mn^{m+}–Mn^{n+} ordering, magnetic measurements do not confirm such a charge ordering.

Experimental Section

$La_{0.5}Sr_{0.5}MnO_{2.5}$ was obtained by the controlled reduction of a sample with the composition $La_{0.5}Sr_{0.5}MnO_3$, which was prepared by a conventional ceramic method reported by Dho et al.[43] The reduction was performed in a CAHN D-200 electrobalance equipped with a furnace and a two-channel register by heating the starting material at 630 °C under an atmosphere containing 200 and 300 mbar of H_2 and He, respectively, at a rate of 6 °C min^{-1}. Once the desired weight loss had been attained, the sample was annealed at 630 °C under He for 24 h to facilitate a more homogeneous distribution of the anionic vacancies. The oxygen content was determined to within $\pm 10^{-3}$ for a sample with a total mass of about 100 mg. Both oxidised and reduced samples were characterised by powder XRD with a Philips X′Pert diffractometer equipped with a $Cu_{K\alpha}$ radiation source. The cationic composition, as determined by XEDS, was found to be in agreement with the nominal one. SAED was performed with a JEOL 2000FX electron microscope fitted with a double tilting goniometer stage (±45°), and HREM was carried out with a JEOL 3000FEG electron microscope fitted with an Oxford LINK EDS analyzer. The sample was dispersed ultrasonically in *n*-butanol and then transferred to holey carbon-coated copper grids. The magnetic properties were determined with a Quantum Design SQUID magnetometer in the temperature range from 5 to 300 K at applied fields of up to 5 T.

Acknowledgments

Financial support from the Ministerio de Educacion y Ciencia for the research project MAT2004-01248 is acknowledged. We thank Dr. K. Boulahya and Dr. E. Matesanz for fruitful discussions.

[1] R. M. von Helmholt, J. Wecker, B. Holzapfel, L. Schultz, K. Samwer, *Phys. Rev. Lett.* **1993**, *71*, 2331–2333.
[2] R. Mahendiran, S. K. Tiwary, A. K. Raychaudhuri, T. V. Ramakrishnan, R. Mahesh, N. Rangavittal, C. N. R. Rao, *Phys. Rev. B* **1996**, *53*, 3348–3358.
[3] J. S. Zhou, J. B. Goodenough, A. Asamitsu, Y. Tokura, *Phys. Rev. Lett.* **1997**, *79*, 3234–3237.
[4] G. Papavassiliou, M. Fardis, M. Belesi, M. Pissas, I. Panagiotopoulos, G. Kallias, D. Niarchos, C. Dimitropoulos, J. Dolinsek, *Phys. Rev. B* **1999**, *59*, 6390–6394.
[5] B. Dabrowski, X. Xiong, R. Dybzinski, P. W. Klamut, J. E. Sieweni, O. Chmaissem, J. Shaffer, C. W. Kimball, *Phys. Rev. B* **1999**, *60*, 7006–7017.
[6] G. Matsumoto, *J. Phys. Soc. Jpn.* **1970**, *29*, 606–615.
[7] J. Alonso, E. Herrero, J. M. González-Calbet, M. Vallet-Regí, J. L. Martínez, J. M. Rojo, A. Hernando, *Phys. Rev. B* **2000**, *62*, 11328–11331.
[8] A. Maignan, C. Simon, V. Caignaert, B. Raveau, *Z. Phys. B* **1996**, *99*, 305–310.
[9] L. M. Rodriguez-Martínez, J. P. Attfield, *Phys. Rev. B* **1996**, *54*, R15622–R15625.
[10] C. Zener, *Phys. Rev.* **1951**, *81*, 440–444; C. Zener, *Phys. Rev.* **1951**, *82*, 403–405.
[11] E. O. Wollan, W. C. Koehler, *Phys. Rev.* **1955**, *100*, 545–563.
[12] J. Rodríguez-Carvajal, M. Hennion, F. Moussa, A. H. Moudden, *Phys. Rev. B* **1998**, *57*, 3189–3192.
[13] C. D. Ling, E. Granado, J. J. Neumeier, J. W. Lynn, D. N. Argyriou. *Phys. Rev. B.* **2003**, *68*, 134439.
[14] J. M. D. Coey, M. Viret, L. Ranno, *Phys. Rev. Lett.* **1995**, *75*, 3910–3913.
[15] A. P. Ramirez, *J. Phys. Condens. Matter* **1997**, *9*, 8171–8199.
[16] C. N. R. Rao, A. Arulraj, P. N. Santosh, A. K. Cheetham, *Chem. Mater.* **1998**, *10*, 2714–2722.
[17] Y. Tomioka, A. Asamitsu, Y. Moritomo, H. Kuwahara, Y. Tokura, *Phys. Rev. Lett.* **1995**, *74*, 5108–5111.
[18] Y. Tomioka, A. Asamitsu, H. Kuwahara, Y. Tokura, *Phys. Rev. B* **1996**, *53*, 1689–1692.
[19] K. Vidyasagar, A. Reller, J. Gopalakrishnan, C. N. R. Rao, *J. Chem. Soc. Chem. Commun.* **1985**, 7–8.
[20] C. N. R. Rao, J. Gopalakrishnan. *Acc. Chem. Res.* **1987**, *20*, 228–235.
[21] A. Reller, D. A. Jefferson, J. M. Thomas, R. A. Beyerlein, K. R. Poeppelmeier, *J. Chem. Soc. Chem. Commun.* **1982**, 1378–1380.
[22] A. Reller, J. M. Thomas, D. A. Jefferson, M. K. Uppal, *Proc. R. Soc. London Ser. A* **1984**, *394*, 223–241.
[23] F. Millange, V. Caignaert, B. Domenges, B. Raveau, *Chem. Mater.* **1998**, *10*, 1974–1983.
[24] L. Er-Rakho, C. Michel, P. Lacorre, B. Raveau, *J. Solid State Chem.* **1998**, *73*, 531–535.
[25] J. M. González-Calbet, E. Herrero, N. Rangavittal, J. M. Alonso, J. L. Martínez, M. Vallet-Regí, *J. Solid State Chem.* **1999**, *148*, 158–168.
[26] G. Q. Gong, C. L. Canedy, G. Xiao, J. Z. Sun, A. Gupta, W. J. Gallagher, *J. Appl. Phys.* **1996**, *79*, 4538–4540.
[27] J. M. Alonso, J. M. González-Calbet, A. Hernando, M. Vallet-Regí, M. E. Dávila, M. C. Asensio, *J. Phys. Chem. Solids* **2006**, *67*, 571–574.
[28] P. S. Casey, D. Barker, A. Hayward, *J. Solid State Chem.* **2006**, *179*, 1375–1382.
[29] R. D. Shannon, *Acta Crystallogr. Sect. A* **1976**, *32*, 751–767.
[30] A. Urishibara, Y. Moritomo, T. Arima, A. Asamitsu, G. Kido, Y. Tokura, *Phys. Rev. B* **1995**, *51*, 14103–14109.
[31] S. W. Cheong, H. Y. Hwang, *Contribution to Colossal Magnetoresistance Oxides in Monographs in Condensed Matter Science* (Ed.: Y. Tokura), Gordon and Breach, London, **1999**.
[32] M. von Harder, H. Müller-Buschbaum, *Z. Anorg. Allg. Chem.* **1980**, *464*, 169–175.
[33] W. T. A. Harrison, T. H. Lee, Y. L. Yang, D. P. Scarfe, L. M. Liu, A. J. Jacobson, *Mater. Res. Bull.* **1995**, *30*, 621–630.
[34] P. Berastegui, S. Hull, F. J. Garcia-Garcia, S. G. Eriksson, *J. Solid State Chem.* **2002**, *164*, 119–130.
[35] V. Y. Pomjakushin, A. M. Balagurov, T. V. Elzhov, D. V. Sheptyakov, P. Fischer, D. I. Khomskii, V. Y. Yushankhai, A. M. Abakumov, M. G. Rozova, E. V. Antipov, M. V. Lobanov, S. J. L. Billinge, *Phys. Rev. B* **2002**, *66*, 184412.

[36] F. Lindberg, S. Y. Istomin, P. Berastegui, G. Svensson, S. M. Kazakov, E. V. Antipov, *J. Solid State Chem.* **2003**, *173*, 395–406.
[37] M. L. Ruiz, C. Prieto, J. Alonso, J. Ramírez-Castellanos, J. M. González-Calbet, *Chem. Mater.* **2002**, *14*, 2055–2062.
[38] M. T. Anderson, K. B. Greenwood, G. A. Taylor, K. R. Poeppelmeier, *Prog. Solid State Chem.* **1993**, *22*, 197–233.
[39] M. Vallet-Regí, E. García, J. M. González-Calbet, *J. Chem. Soc. Dalton Trans.* **1988**, 775–779.
[40] P. Marchukov, R. Geick, C. Brotzeller, W. Treutmann, E. G. Rudashevsky, A. M. Balbashov, *Phys. Rev. B* **1993**, *48*, 13538–13546.
[41] A. Sundaresan, P. L. Paulose, R. Mallik, E. V. Sampathkumaran, *Phys. Rev. B* **1998**, *57*, 2690–2693.
[42] S. V. Trukhanov, N. V. Kasper, I. O. Troyanchuk, M. Tovar, H. Szymczak, K. Bärner, *J. Solid State Chem.* **2002**, *169*, 85–95.
[43] J. Dho, W. S. Kim, N. H. Hur, *Phys. Rev. Lett.* **2001**, *87*, 187201.

Received: September 5, 2006
Revised: November 16, 2006
Published online: January 17, 2007

